Coherent Gate Operations in Hybrid Magnonics

Jing Xu, Changchun Zhong, Xu Han, Dafei Jin, Liang Jiang, and Xufeng Zhang

Phys. Rev. Lett. **126**, 207202 — Published 21 May 2021

DOI: 10.1103/PhysRevLett.126.207202

Coherent Gate Operations in Hybrid Magnonics

Jing Xu,[1] Changchun Zhong,[2] Xu Han,[1] Dafei Jin,[1] Liang Jiang,[2] and Xufeng Zhang[1,*]

[1]*Center for Nanoscale Materials, Argonne National Laboratory, Lemont, IL 60439, USA*
[2]*Pritzker School of Molecular Engineering, University of Chicago, Chicago, IL 60637, USA*

(Dated: April 22, 2021)

Electromagnonics—the hybridization of spin excitations and electromagnetic waves—has been recognized as a promising candidate for coherent information processing in recent years. Among its various implementations, the lack of available approaches for real-time manipulation on the system dynamics has become a common and urgent limitation. In this work, by introducing a fast and uniform modulation technique, we successfully demonstrate a series of benchmark coherent gate operations in hybrid magnonics, including semi-classical analogy of Landau-Zener transition, Rabi oscillation, Ramsey interference, and controlled mode swap operation. Our approach lays the groundwork for dynamical manipulation of coherent signals in hybrid magnonics, and can be generalized to a broad range of applications.

With the ever-growing complexity of modern signal processing techniques, there are rapidly increasing interests nowadays in integrating different physical platforms, accordingly different types of information carriers, onto a single device. Such systems, often referred to as hybrid systems [1], can enable comprehensive functionalities that are otherwise challenging to achieve on any individual physical platforms. Among various hybrid systems, hybrid magnonics [2–6] has been attracting intensive attention recently because of its distinct advantages. In hybrid magnonics, information is processed by the coherent interaction between magnons – quanta of collective spin excitations known as spin waves – and other forms of information carriers such as microwave photons [7–12], optical photons [13–17], and mechanical phonons [18, 19]. Hybrid magnonic systems based on magnetic insulator yttrium iron garnet (YIG) exhibit a series of unique properties such as large frequency tunability, enhanced coupling strength, excellent compatibility, etc., offering great potential for coherent information transduction.

The most well-developed hybrid magnonic system today is electromagnonics, which focuses on coherent interactions between coupled magnonic and microwave resonators [7–12]. Magnon-microwave photon strong coupling achieved in such systems enable novel phenomena and applications in both classical and quantum regimes, including non-reciprocal signal routing [20–22], non-Hermitian physics [23, 24], microwave-to-optical transduction [17, 25], quantum magnonics [26–28], dark matter detection [29, 30], etc. Nevertheless, in these demonstrations the electromagnonic interaction can only be tuned by changing the geometric configuration of the device, which typically occurs on a time scale much longer than the signal lifetime. The lack of fast tuning mechanisms makes it extremely challenging to apply any gate-control protocols [31–42] for real-time manipulations on the magnon-photon interaction dynamics which is highly desired for practical signal processing, severely limiting the broad application of electromagnonic systems.

In this Letter, we demonstrate that by introducing a novel pulse sequence [43] gated electromagnonic interactions are achieved, to the best of our knowledge, for the first time. Our gate design ensures fast response time to the control pulses, which is hardly achievable in previous demonstrations. This allows the control of the on, off, and duration of the magnon-photon interaction to realize a series of gated dynamics, including semi-classical analogy of Landau-Zener (LZ) transition, Rabi oscillation, Ramsey interference, and controlled swap. Upon further optimization to extend the finite magnon/photon lifetimes and magnon detuning range, more complicated operations are expected. Our proof-of-principle demonstration opens a new avenue for dynamically manipulating electromagnonic systems.

Figure 1 (a) shows the schematics of our device, consisting of a cylinder-shaped dielectric resonator (DR) hosted inside a large copper housing (not shown for clarity). The DR supports a well-defined photon mode ($\mathrm{TE}_{01\delta}$ mode) at $\omega_c = 2\pi \times 8.517$ GHz with a small dissipation (quality factor around 10,000) thanks to the low dielectric loss as well as the radiation shielding from the housing. The resonator volume (diameter: 6 mm; height: 4 mm) is much smaller than metallic three-dimensional cavities [7, 8, 10] at similar frequencies because of its high dielectric constant ($\varepsilon = 30$). One coaxial loop antenna (the "probe") is placed on top of the DR to excite cavity microwave photons. This antenna also reads out the coherent information encoded on the amplitude and phase of cavity photons, either by steady-state cavity reflection spectra under a continuous wave (CW) RF excitation, or via cavity dynamical responses under a pulsed excitation.

A 400-μm-diameter sphere made of single crystal YIG is placed close to the end surface of the DR along its axis. A permanent magnet is placed outside the cavity housing to provide a bias field along z direction to magnetize the YIG sphere. The bias field direction is perpendicular to the microwave magnetic field of the DR $\mathrm{TE}_{01\delta}$ mode [dashed lines along y direction in Fig. 1 (a)], inducing the coupling between magnon resonances in the YIG sphere and the evanescent field of the cavity resonance. The bias field strength H is controlled by the permanent magnet position. In our experiment, only the fundamental magnon mode is considered, which has a frequency determined as $\omega_m = \gamma H$, where $\gamma = 2\pi \times 28$ GHz/T is the gyromagnetic ratio.

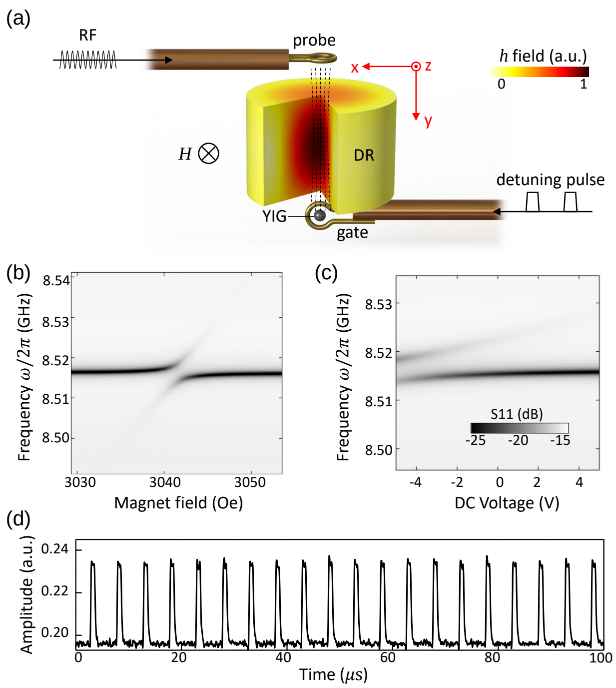

FIG. 1. (a) Device schematics. A spherical YIG magnonic resonator is placed underneath a cylindrical dielectric resonator (DR) inside a copper housing (not shown for clarity). An external magnetic field H is applied along z by a permanent magnet. The probe loop is for microwave excitation/readout; the gate loop around the YIG sphere provides control fields along z using pulsed DC currents. The gate loop is optimized to three turns in the real device, but only a single turn is plotted for clarity. The colormap and vertical dashed lines show the amplitude and direction of the microwave magnetic (h) fields of the DR $\mathrm{TE}_{01\delta}$ mode. (b),(c) Measured cavity reflection (S_{11}) spectra when the bias magnetic field and gate voltage is swept, respectively. (d) Pulse response of the on-resonance cavity reflection when a train of 800-ns, 10-V_{pp} DC pulses with a repetition rate of 200 kHz is applied to the gate.

Our system can be described by the Hamiltonian

$$\hat{H} = \hbar\omega_{\mathrm{c}}\hat{c}^{\dagger}\hat{c} + \hbar\omega_{\mathrm{m}}\hat{m}^{\dagger}\hat{m} + \hbar g\left(\hat{c}^{\dagger}\hat{m} + \hat{c}\hat{m}^{\dagger}\right), \tag{1}$$

where $\hbar$ is the reduced Planck's constant, g is the magnon-photon coupling strength, $\hat{c}$ and $\hat{c}^{\dagger}$ ($\hat{m}$ and $\hat{m}^{\dagger}$) are the annihilation and creation operators for the photon (magnon) mode, respectively. In our experiment, strong magnon-photon coupling is achieved [Fig. 1 (b)] thanks to the large spin density in YIG as well as the photon recycling in the DR near resonance, allowing coherent information conversion between the two modes. The lower and upper branch correspond to hybrid modes where the magnons and photons are in-phase and out-of-phase, respectively, which give $\hat{d}_{\pm} = (\hat{c} \pm \hat{m})/\sqrt{2}$ at zero detuning ($\omega_{\mathrm{c}} = \omega_{\mathrm{m}}$) with the $+(-)$ sign for the lower (upper) branch. Strong coupling is confirmed by the extracted parameters, with a coupling strength $g = 2\pi \times 2.25$ MHz exceeding both the photon and magnon dissipation rates ($\kappa_{\mathrm{c}} = 2\pi \times 0.96$ MHz and $\kappa_{\mathrm{m}} = 2\pi \times 1.20$ MHz), which correspond to a lifetime of 166 ns and 133 ns, respectively.

A unique feature of our device is a gate antenna [44] wrapping around the YIG sphere, allowing bias field tuning with a DC current [Fig. 1 (c)]. The loop has a small diameter (900 μm) to enhance the tuning field, and with only three turns its inductance is also small, allowing fast responds to short current pulses. During their "on" times, such pulses can detune the magnon resonance and are therefore referred to as detuning pulses. For example, when a 10-Vpp pulse train (pulse length: 800 ns, repetition rate: 200 kHz) is sent to the gate, the measured cavity reflection of a CW tone at $2\pi \times 8.5185$ GHz is modulated into a pulse train [Fig. 1 (d)]. Therefore, dynamical control of the system response becomes feasible.

The transient response of the system is characterized using a pulse sequence shown in Fig. 2 (a). The gate current is first set to zero by a 0-V gate voltage and the permanent magnet is tuned to have the magnon mode on resonance with the cavity. This is followed by a -5-V gate voltage to bring the magnon mode off resonance. Then a 100-ns RF pulse centered at ω_{c} is sent to the probe to excite the system. Since the RF probe only couples with the cavity mode, the system is excited into a nearly pure photon state. After that a detuning pulse brings the bias voltage from -5 V to $+5$ V, sweeping magnons across the cavity resonance with a $\pm 2\pi \times 5.75$ MHz detuning range. Cavity reflection is read out right after the rise edge of the detuning pulse, which is a direct indication of the cavity mode amplitude. During the readout, the DC bias stays at $+5$ V for 500 ns to keep the system in the steady state. The pulse repetition time (2 μs) is much longer than the pulse sequence.

In the strong coupling regime, the cavity photon and magnon mode hybridize into two normal modes with one upper and one lower branch that are separated by an anti-crossing [Fig. 2 (b)]. In our measurement, the transition time t_{LZ} for the gate voltage to change from -5 V to $+5$ V is tuned from 6 to 200 ns, determining different evolution paths for the system initial state. For a large t_{LZ}, the initial state undergoes an adiabatic transition (Path P_1) and stays in the upper branch, during which cavity photons gradually convert to the magnon mode. While for a small t_{LZ}, the initial state experiences a diabatic transition (Path P_2) and jumps from the upper to the lower branch, allowing cavity photons to remain in the photon mode. For other transitions that fall between these two limits, cavity photons will take both paths with a probability of remaining in the photon mode

$$P_{\mathrm{c}} = e^{\frac{-\pi g^2}{\Delta\omega_{\mathrm{m}}/t_{\mathrm{LZ}}}}, \tag{2}$$

which is analogous to the LZ transition in atomic physics [45]. In our system, the magnon detuning at both the initial and final states satisfies $|\Delta\omega_{\mathrm{m}}| = |\omega_{\mathrm{m}} - \omega_{\mathrm{c}}| = 2\pi \times 5.75$ MHz $> g/2$, validating the adoption of the LZ formula [46].

The cavity mode amplitude is characterized by measuring the cavity reflection as a function of the LZ transition time. The cavity reflection is proportional to the strength of the electromagnetic field inside the cavity, thus directly indicates the intra-cavity photon dynamics. The finite microwave photon lifetime has to be taken into account considering it

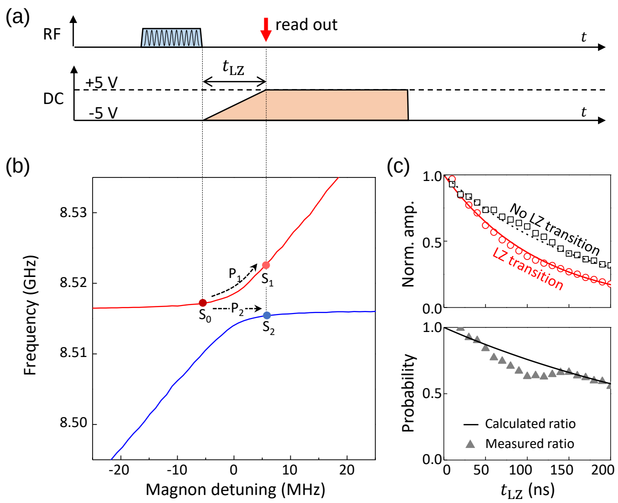

FIG. 2. (a) Schematics of the pulse sequence used for measuring the Landau-Zener (LZ) transition. A 10-V_{pp} detuning pulse with a rise edge t_{LZ} and peak duration 500 ns is applied right after the 100-ns input microwave pulse. Cavity reflection is read out right after the detuning pulse rise edge (red arrow). (b) Measured normal mode frequencies of the hybrid magnonic system. S_0 is the initial state after the pulsed RF excitation, $P_{1,2}$ and $S_{1,2}$ are the possible transition paths and the corresponding final states, respectively. (c) Normalized amplitude (norm. amp.) for the cavity mode measured after the detuning pulse as a function of t_{LZ} with (circles) and without LZ transition (squares), respectively. Solid and dashed lines are the calculation results for these two situations, respectively. Bottom panel: Measured (triangles) and calculated (solid line) ratio of the amplitudes with and without the LZ transition.

is on a time scale similar to the LZ transition time. Consequently, the normalized cavity mode amplitude is given as $A = P_c e^{-\kappa_c t_{LZ}}$. Figure 2 (c) shows both measured (red circles) and calculated (red solid line) cavity mode amplitudes, which show great agreement with each other. As a comparison, Figure 2 (c) also plots the measured (black squares) and calculated (dashed line) photon decays resulting solely from the cavity dissipation when magnons are detuned far away from cavity resonance, which show a much lower exponential decay rate and are therefore distinctively different from the LZ transition case.

The bottom panel of Fig. 2 (c) shows that the derived probability P_c also agrees with the calculation based on Eq. (2). For longer transition times, the probability for the photons to stay in the cavity resonance is low, e.g., $P_c = 0.57$ for $t_{LZ} = 200$ ns. However, for rapid LZ transitions the system condition can be abruptly changed (e.g., magnons to be quickly tuned on/off-resonance) without affecting existing states. For instance, photons have a high probability $P_c = 0.98$ to stay in the microwave resonance after the transition for $t_{LZ} = 6$ ns. In our system, the device can be first excited into a pure photon state $\psi(0) = |\alpha\rangle_c |0\rangle_m$, where $|\alpha\rangle_c$ and $|0\rangle_m$ are coherent states for the photon (amplitude: α) and magnon (amplitude: 0) mode, respectively, by a RF pulse centered at ω_c when magnons are far off resonance ($|\Delta\omega_m| > g/2$). Without detuning pulses,

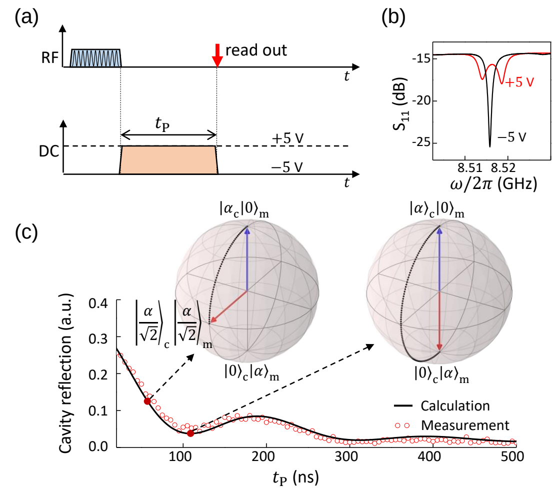

FIG. 3. (a) Schematics of the pulse sequence for measuring the Rabi oscillation. A 10-V_{pp}, rectangular-shaped Rabi pulse is applied after the 100-ns microwave input pulse. The detuning pulse has a rise/fall edge of 6 ns, with a varying pulse length t_R. Cavity reflection is read out right after the Rabi-pulse. (b) Red (black) line shows cavity reflection spectrum at the pulse peak (bottom), where magnons are on (off) resonance with cavity photons. (c) Measured (red open circles) and calculated (black solid line) time trace of the cavity reflection signal as a function of the Rabi pulse length t_R, respectively. Inset shows the Bloch sphere representation of the system state evolution after a 56-ns (left) and 111-ns (right) pulse which serve as a $\pi/2$- and a π-pulse, respectively. α is the initial photon mode amplitude.

the system dynamics is simply an exponential decay. When a detuing pulse with a short rise/fall time and proper amplitude is applied, the initial photon state stays intact but the magnon mode can be abruptly tuned to be on-resonance with cavity photons during the finite pulse length t_p. This enables the information conversion between photons and magnons within the pulse duration, and consequently the system state evolves to

$$\psi(t_p) = |\alpha \cos(g t_p)\rangle_c \, |\alpha \sin(g t_p)\rangle_m . \qquad (3)$$

Therefore, by properly tuning the pulse length the system final state can be controlled. For instance, if $t_p = T_R/2$ where $T_R = \pi/g$ is the Rabi period, the final state of the system becomes $|0\rangle_c |\alpha\rangle_m$ if the dissipation is neglected. Such a pulse swaps the magnon mode with the cavity photon mode, and therefore corresponds to a π-pulse. Accordingly, a $\pi/2$-pulse can be obtained if the pulse length becomes $t_p = T_R/4$, which converts a pure photon state into a hybrid state $|\alpha/\sqrt{2}\rangle_c |\alpha/\sqrt{2}\rangle_m$ [44].

Our experimental realization of gate controls is depicted in Fig. 3 (a). First the system is initialized with a −5-V gate signal, and the bias magnet is adjusted to detune the magnon mode from the cavity resonance by $2\pi \times 11.5$ MHz [Fig. 3 (b)]. Then a 100-ns, rectangular-shaped microwave pulse centered at ω_c is sent in and excites the system into a photon mode. When the microwave pulse ends, a detuning pulse with a rise/fall edge of 6 ns is applied immediately to abruptly increase the DC bias to +5 V, bringing the magnon mode

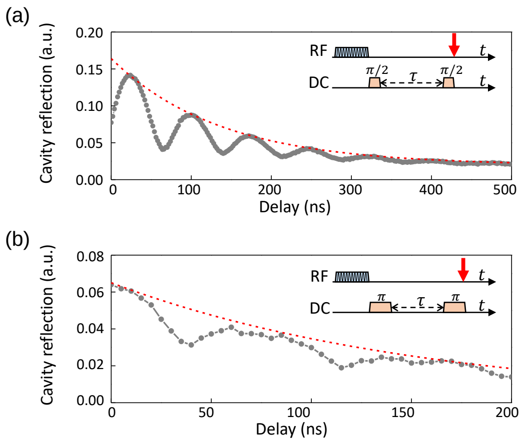

FIG. 4. (a) Measured Ramsey fringe using the pulse sequence shown in the inset with two 10-V_{pp} $\pi/2$-pulses separated by τ. (b) Measured cavity reflection signal after a mode swap operation using the pulse sequence shown in the inset with two 10-V_{pp} π-pulses separated by τ. In both measurements, the first detuning pulse is applied immediately after the 100-ns RF excitation pulse, and the cavity reflection is read-out (at red arrows) right after the second pulse.

on-resonance with cavity photons [Fig. 3 (b)]. The detuning pulse lasts for t_p before the bias returns to -5 V, after which the cavity reflection is read out. When the detuning pulse length t_p varies, a Rabi oscillation is observed [red open circles in Fig. 3 (c)], which agrees well with theoretical prediction (black solid line) based on Eq. (3). From these results a Rabi period of $T_R = 222$ ns can be extracted, which perfectly matches the measured coupling strength $g = 2\pi \times 2.25$ MHz. Consequently, a 56-ns and a 111-ns pulse correspond to a $\pi/2$- and a π-pulse, respectively, as indicated by the Bloch sphere representation [Fig. 3 (c), inset].

Based on the effective $\pi/2$- and π-pulses, complex electromagnonic gate controls can be realized using multi-pulse sequences. For instance, Ramsey fringes, which have been widely adopted for characterizing dephasing processes, can be measured using a pair of $\pi/2$-pulses [Fig. 4(a)]. First the system is prepared with the magnon mode detuned by $2\pi \times 11.5$ MHz at a -5-V bias voltage, followed by a microwave pulse exciting the system into a pure photon state. The first $\pi/2$-pulse (amplitude: $+5$ V) is then applied to convert microwave photons into the hybrid mode $|\alpha/\sqrt{2}\rangle_c |\alpha/\sqrt{2}\rangle_m$. After a delay τ in which the hybrid mode undergoes a free evolution, the second $\pi/2$-pulse is applied. Cavity reflection is immediately read out after the second pulse, which shows an oscillation as a function of τ with a period (79 ns) close to the theoretical prediction $T_{\text{Ramsey}} = 2\pi/\Delta\omega_m = 87$ ns. An exponential fitting of its envelop gives a lifetime of 136 ns, slightly smaller than the expected decay time (147 ns) determined from the hybrid mode damping rate $\kappa_\pm = (\kappa_c + \kappa_m)/2 = 2\pi \times 1.08$ MHz, indicating that for the hybrid modes the dephasing process is comparable with but slightly faster than their damping.

In addition, controlled magnon-photon mode swap can be obtained using a π-π pulse sequence [Fig. 4(b)]. This is in sharp contrast to most previous demonstrations where the magnon-photon swap is constantly on without any controls. With the system initially prepared in a pure photon state as in the Ramsey fringe measurement, it is swapped into the magnon state by a π-pulse. As the pulse ends magnons are tuned off-resonance, leaving the information in the magnon state. The second π-pulse after a delay τ enables a second swap, converting the information back to the photon mode. The converted signal amplitude experiences an exponential decay [Fig. 4(b)], which is determined by the magnon damping. Limited by the finite magnon detuning that we can achieve, the magnon-photon interaction is not completely turned off after the π-pulse, which explains the slight oscillatory deviation from ideal situations (dashed line) in the measured signal. Although it may not be ideal for memory applications because of the finite magnon lifetime, the demonstrated principle can be used for on-demand mode conversions that are long desired in many other applications.

To conclude, we have achieved the first real-time gate control of coherent magnon-photon interactions. Using a tuning mechanism that supports fast pulse responses, we successfully obtained the proof-of-principle demonstration for several benchmark gated magnon-photon operations. Our demonstration points to a new direction for hybrid magnonics where magnon-photon couplings have been long limited to be static or quasi-static, opening new possibilities for a broad range of applications in coherent information processing. Upon further optimizations to extend the finite photon/magnon lifetimes and detuning ranges, our room-temperature, classical demonstrations can be readily applied to low-temperature, quantum measurements.

This work was performed, in part, at the Center for Nanoscale Materials, a U.S. Department of Energy Office of Science User Facility, and supported by the U.S. Department of Energy, Office of Science, under Contract No. DE-AC02-06CH11357. L.J. acknowledges support from the ARL-CDQI (W911NF-15-2-0067), ARO (W911NF-18-1-0020, W911NF-18-1-0212), ARO MURI (W911NF-16-1-0349), AFOSR MURI (FA9550-15-1-0015, FA9550-19-1-0399), NSF (EFMA-1640959, OMA-1936118), and the Packard Foundation (2013-39273).

* xufeng.zhang@anl.gov

[1] G. Kurizki, P. Bertet, Y. Kubo, K. Mlmer, D. Petrosyan, P. Rabl, and J. Schmiedmayer, Proc. Natl. Acad. Sci. **112**, 3866 (2015).
[2] M. Harder and C.-M. Hu, Solid State Phys. **69**, 47 (2018).
[3] D. Lachance-Quirion, Y. Tabuchi, A. Gloppe, K. Usami, and Y. Nakamura, Appl. Phys. Express **12**, 070101 (2019).
[4] B. Bhoi and S.-K. Kim, Solid State Phys. **71**, 39 (2020).
[5] Y. Li, W. Zhang, V. Tyberkevych, W.-K. Kwok, A. Hoffmann, and V. Novosad, J. Appl. Phys. **128**, 130902 (2020).
[6] D. D. Awschalom, C. H. R. Du, R. He, F. J. Heremans, A. Hoffmann, J. Hou, H. Kurebayashi, Y. Li, L. Liu, V. Novosad, J. Sklenar, S. E. Sullivan, D. Sun, H. Tang, V. Tiberkevich, C. Trevillian, A. W. Tsen, L. R. Weiss, W. Zhang, X. Zhang,

L. Zhao, and C. W. Zollitsch, arXiv:2102.03222 (2021).

[7] X. Zhang, C.-L. Zou, L. Jiang, and H. X. Tang, Phys. Rev. Lett. **113**, 156401 (2014).

[8] Y. Tabuchi, S. Ishino, T. Ishikawa, R. Yamazaki, K. Usami, and Y. Nakamura, Phys. Rev. Lett. **113**, 083603 (2014).

[9] M. Goryachev, W. Farr, D. Creedon, Y. Fan, M. Kostylev, and M. Tobar, Phys. Rev. Appl. **2**, 054002 (2014).

[10] L. Bai, M. Harder, Y. Chen, X. Fan, J. Xiao, and C.-M. Hu, Phys. Rev. Lett. **114**, 227201 (2015).

[11] Y. Li, T. Polakovic, Y.-L. Wang, J. Xu, S. Lendinez, Z. Zhang, J. Ding, T. Khaire, H. Saglam, R. Divan, J. Pearson, W.-K. Kwok, Z. Xiao, V. Novosad, A. Hoffmann, and W. Zhang, Phys. Rev. Lett. **123**, 107701 (2019).

[12] J. T. Hou and L. Liu, Phys. Rev. Lett. **123**, 107702 (2019).

[13] A. Osada, R. Hisatomi, A. Noguchi, Y. Tabuchi, R. Yamazaki, K. Usami, M. Sadgrove, R. Yalla, M. Nomura, and Y. Nakamura, Phys. Rev. Lett. **116**, 223601 (2016).

[14] X. Zhang, N. Zhu, C.-L. Zou, and H. X. Tang, Phys. Rev. Lett. **117**, 123605 (2016).

[15] J. Haigh, A. Nunnenkamp, A. Ramsay, and A. Ferguson, Phys. Rev. Lett. **117**, 133602 (2016).

[16] S. V. Kusminskiy, H. X. Tang, and F. Marquardt, Phys. Rev. A **94**, 033821 (2016).

[17] N. Zhu, X. Zhang, X. Han, C. Zou, C. Zhong, C. Wang, L. Jiang, and H. Tang, Optica **7**, 1291 (2020).

[18] X. Zhang, C.-L. Zou, L. Jiang, and H. X. Tang, Sci. Adv. **2**, e1501286 (2016).

[19] K. An, A. N. Litvinenko, R. Kohno, A. A. Fuad, V. V. Naletov, L. Vila, U. Ebels, G. de Loubens, H. Hurdequint, N. Beaulieu, J. B. Youssef, N. Vukadinovic, G. E. W. Bauer, A. N. Slavin, V. S. Tiberkevich, and O. Klein, Phys. Rev. B **101**, 060407(R) (2020).

[20] Y.-P. Wang, J. Rao, Y. Yang, P.-C. Xu, Y. Gui, B. Yao, J. You, and C.-M. Hu, Phys. Rev. Lett. **123**, 127202 (2019).

[21] X. Zhang, A. Galda, X. Han, D. Jin, and V. M. Vinokur, Phys. Rev. Appl. **13**, 044039 (2020).

[22] N. Zhu, X. Han, C.-L. Zou, M. Xu, and H. X. Tang, Phys. Rev. A **101**, 043842 (2020).

[23] D. Zhang, X.-Q. Luo, Y.-P. Wang, T.-F. Li, and J. Q. You, Nat. Commun. **8**, 1368 (2017).

[24] X. Zhang, K. Ding, X. Zhou, J. Xu, and D. Jin, Phys. Rev. Lett. **123**, 237202 (2019).

[25] R. Hisatomi, A. Osada, Y. Tabuchi, T. Ishikawa, A. Noguchi, R. Yamazaki, K. Usami, and Y. Nakamura, Phys. Rev. B **93**, 174427 (2016).

[26] Y. Tabuchi, S. Ishino, A. Noguchi, T. Ishikawa, R. Yamazaki, K. Usami, and Y. Nakamura, Science **349**, 405 (2015).

[27] D. Lachance-Quirion, S. P. Wolski, Y. Tabuchi, S. Kono, K. Usami, and Y. Nakamura, Science **367**, 425 (2020).

[28] S. P. Wolski, D. Lachance-Quirion, Y. Tabuchi, S. Kono, A. Noguchi, K. Usami, and Y. Nakamura, Phys. Rev. Lett. **125**, 117701 (2020).

[29] G. Flower, J. Bourhill, M. Goryachev, and M. Tobar, Phys. Dark Universe **25**, 100306 (2019).

[30] T. Trickle, Z. Zhang, and K. M. Zurek, Phys. Rev. Lett. **124**, 201801 (2020).

[31] P. Krantz, M. Kjaergaard, F. Yan, T. P. Orlando, S. Gustavsson, and W. D. Oliver, Appl. Phys. Rev. **6**, 021318 (2019).

[32] M. Hirose and P. Cappellaro, Nature **532**, 77 (2016).

[33] J. L. O'Brien, G. J. Pryde, A. G. White, T. C. Ralph, and D. Branning, Nature **426**, 264 (2003).

[34] N. W. Hendrickx, D. P. Franke, A. Sammak, M. Kouwenhoven, D. Sabbagh, L. Yeoh, R. Li, M. L. V. Tagliaferri, M. Virgilio, G. Capellini, G. Scappucci, and M. Veldhorst, Nat. Commun. **9**, 2835 (2018).

[35] A. Crippa, R. Ezzouch, A. Apra, A. Amisse, R. Lavieville, L. Hutin, B. Bertrand, M. Vinet, M. Urdampilleta, T. Meunier, M. Sanquer, X. Jehl, R. Maurand, and S. D. Franceschi, Nat. Commun. **10**, 2776 (2019).

[36] E. Kawakami, T. Jullien, P. Scarlino, D. R. Ward, D. E. Savage, M. G. Lagally, V. V. Dobrovitski, M. Friesen, S. N. Coppersmith, M. A. Eriksson, and L. M. K. Vandersypen, Proc. Natl. Acad. Sci. U.S.A. **113**, 11738 (2016).

[37] D. B. Bucher, D. P. L. A. Craik, M. P. Backlund, M. J. Turner, O. B. Dor, D. R. Glenn, and R. L. Walsworth, Nat. Protoc. **14**, 2707 (2019).

[38] M. K. Bhaskar, R. Riedinger, B. Machielse, D. S. Levonian, C. T. Nguyen, E. N. Knall, H. Park, D. Englund, M. Loncar, D. D. Sukachev, and M. D. Lukin, Nature **580**, 60 (2020).

[39] R. C. C. Leon, C. H. Yang, J. C. C. Hwang, J. C. Lemyre, T. Tanttu, W. Huang, K. W. Chan, K. Y. Tan, F. E. Hudson, K. M. Itoh, A. Morello, A. Laucht, M. Pioro-Ladriere, A. Saraiva, and A. S. Dzurak, Nat. Commun. **11**, 797 (2020).

[40] J. Wong-Campos, S. Moses, K. Johnson, and C. Monroe, Phys. Rev. Lett. **119**, 230501 (2017).

[41] L. Casparis, T. Larsen, M. Olsen, F. Kuemmeth, P. Krogstrup, J. Nygard, K. Petersson, and C. Marcus, Phys. Rev. Lett. **116**, 150505 (2016).

[42] J. M. Chow, L. DiCarlo, J. M. Gambetta, F. Motzoi, L. Frunzio, S. M. Girvin, and R. J. Schoelkopf, Phys. Rev. A **82**, 040305(R) (2010).

[43] B. T. Torosov and N. V. Vitanov, Phys. Rev. A **99**, 013424 (2019).

[44] Supplemental Material.

[45] J. R. Rubbmark, M. M. Kash, M. G. Littman, and D. Kleppner, Phys. Rev. A **23**, 3107 (1981).

[46] M. P. Silveri, J. A. Tuorila, E. V. Thuneberg, and G. S. Paraoanu, Rep. Prog. Phys. **80**, 056002 (2017).